Patient-specific optimization of mechanical ventilation for patients with acute respiratory distress syndrome using quasi-static pulmonary P-V data

Mohsen Nabian[a,*], Uichiro Narusawa[a,b]

[a] Department of Mechanical and Industrial Engineering, Northeastern University, Boston, MA, USA
[b] Department of Bio-engineering, Northeastern University, Boston, MA, USA

ARTICLE INFO

ABSTRACT

Quasi-static, pulmonary pressure-volume (P-V) curves were combined with a respiratory system model to analyze tidal pressure cycles, simulating mechanical ventilation of patients with acute respiratory distress syndrome (ARDS). Two important quantities including 1) tidal recruited volume and 2) tidal hyperinflated volume were analytically computed by integrating the distribution of alveolar elements over the affected pop-open pressure range. We analytically predicted the tidal recruited volume of four canine subjects and compared our results with similar experimental measurements on canine models for the validation. We then applied our mathematical model to the P-V data of ARDS populations in four stages of Early ARDS, Deep Knee, Advanced ARDS and Baby Lung to quantify the tidal recruited volume and tidal hyperinflated volume as an indicator of ventilator-induced lung injury (VILI). These quantitative predictions based on patient-specific P-V data suggest that the optimum parameters of mechanical ventilation including PEEP and Tidal Pressure (Volume) are largely varying among ARDS population and are primarily influenced by the degree in the severity of ARDS.

1. Introduction

Since the early definition of acute respiratory distress syndrome (ARDS), a multitude of clinical studies have been published on such subjects as the use of pressure-volume (P-V) curves for mechanical ventilation of patients with ARDS [22,23,35,36,46,58,66], PEEP (positive end-expiratory pressure) vs. ZEEP (zero end-expiratory pressure) and a degree of PEEP for effective ventilation [4,10,15,19–21,27,29,31,37–39,45,47,49,50,60]. Also large-scale ARDS ventilation trials [14,34,43] were conducted to investigate effective mechanical ventilation strategies to prevent hyperinflation and ventilator-induced-lung injury (VILI) [13,17,24,48,51,56,57,61,69] while maintaining sufficient oxygenation. Although these experimental studies have significantly contributed to the optimization of mechanical ventilation and thus the decrease in the mortality rate of ARDS patients, majority of these studies investigated for "one-size-fits-all" values of PEEP and tidal volume for the entire ARDS population [8,11]. This generalization is criticized by many studies [10,19,24,38,39,45,50,60] that suggest patient-specific PEEP and tidal volume values for the optimization of mechanical ventilation.

Analytical modelings of respiratory system were investigated in Refs. [59] and [9] by developing a statistical model of the inflation process with a power-law distribution of the airway openings. Since

then, the modeling studies of the respiratory system and/or the mechanical ventilation include a non-linear circuit model for the mechanical ventilation [47], an application of a sigmoidal P-V equation [65] to optimize the mechanical ventilation [41,60], an examination of lung compliance during the mechanical ventilation [27], and a development of a recruitment function from the P-V curve [32]. Many previous investigations [10,18,19,24,38,39,45,50,54,60] also pointed out needs for balancing alveolar recruitment and hyperinflation as well as for information on ventilation strategy more applicable to individuals than to population.

In Refs. [40,42], quasi-static pulmonary P-V curves along with a respiratory system model developed in Refs. [5–7] were analyzed for the patients with ARDS, canine models and healthy humans to propose four stages of ARDS.

In this paper we aimed to contribute to the researches in the optimization of mechanical ventilation by combining the quasi-static pulmonary P-V curves of individuals with the respiratory system model developed in Refs. [5–7] to further analyze mechanical ventilation of ARDS patients under the hypothesis that our respiratory system model yields quantitative prediction of tidal recruited volume and tidal hyperinflated volume.

We first analytically predicted the tidal recruited volume of four canine subjects as function of PEEP and compared our results with a

---

similar experimental measurements on canine models. We then applied our mathematical model to four stages of ARDS (Early ARDS, Deep Knee, Advanced ARDS and Baby Lung) defined in Ref. [42] to quantify the tidal recruited volume and tidal hyperinflated volume. Our quantitative predictions of these two parameters in various ARDS patients suggest that the optimum parameters of mechanical ventilation including PEEP and Tidal Pressure (or Tidal Volume) are largely varying among ARDS population and are primarily influenced by the degree in the severity of ARDS.

2. Background

2.1. Respiratory system model (RSM)

A proposed P-V model equation [5–7] in the form of error-function is (See Fig. 1(c)):

$$V = V_U - \frac{\Delta V}{2} + \frac{\Delta V}{2} \cdot erf\left(\frac{\sqrt{\pi}}{4}\Lambda \cdot \left(\frac{P}{P_0} - 1\right)\right)$$

(1)
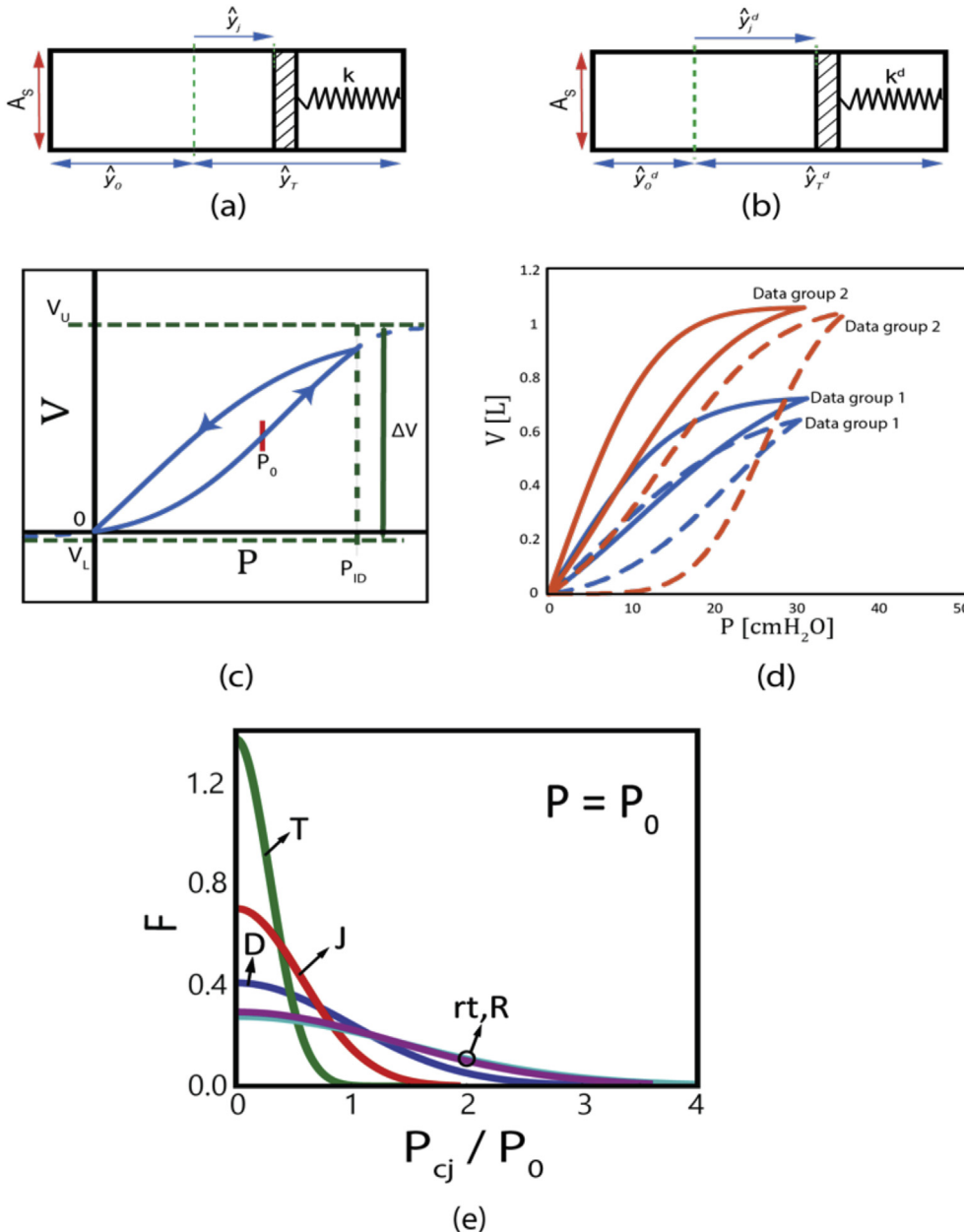
Fig. 1. (a) Alveolar element for inflation: The element pops-open as its pressure exceeds the P_{cj}. $A_s\hat{y}_0 = \hat{V}_0$ (pop-open volume of an element), $A_s\hat{y}_T = \hat{V}_{distension}$ (volume increase due to elastic wall distension). (b) Alveolar element for deflation. Superscript, d, indicates properties of deflation. (c) Quasi-static inflation-deflation P-V curve. V_U = upper volume asymptote (total lung capacity), V_L = lower volume asymptote, ΔV $(=V_U - V_L)$ = vital lung capacity, P_0 = pressure at the midpoint of P-V curve, P_{ID} = pressure at the intersection of inflation- and deflation-curve. (d) P-V curves of Data group 1 and Data group 2 (solid = Before Injury, dotted = After Injury). (e) Normalized distribution of alveolar elements at $P = P_0$. Data sets D, J, R, T of Data group 3 (ARDS) and Data set rt of Data group 5 (healthy human).

where four parameters are $V_U=$ the upper asymptote (total lung capacity (TLC)), $\Delta V (= V_U - V_L)$ = vital lung capacity (VLC) with $V_L=$ the lower asymptote (functional residual capacity (FRC))), $P_0=$ pressure at the midpoint (inflection point) of the P-V curve, and the non-dimensional parameter, Λ, with the error-function, $erf(x)$, defined as, $erf(x) = (2/\sqrt{\pi})\int_0^x e^{-t^2}dt$, $erf(\infty) = 1$, $erf(-x) = -erf(x)$. The deflation P-V curves are also represented by Eq. (1) with the four inflation parameters replaced by the corresponding deflation parameters of V_U^d, ΔV^d, P_0^d and Λ^d. (See Fig. 1(d) for various inflation-deflation loops.)

Presented below is an outline of our (respiratory system) model and its relation to the P-V model equation [6]. A total respiratory system is represented by a large population of alveolar elements (N = total number of elements) distributed over its (alveolar) opening pressure P_{cj}. Referring to Fig. 1(a), an element, j, consists of a cylindrical chamber with a piston-spring system ($A_s=$ piston surface area, $k=$ spring constant [N/m], $\hat{y}_0=$ piston displacement due to pop-open mechanism, $\hat{y}_T=$ piston displacement due to elastic wall distension). The element is closed when the piston is located at the left end of the cylinder. Once the pressure acting on the left hand side of the piston reaches P_{cj}, the piston moves to a new position of $\hat{y}_0$ ('pop-open' mechanism = alveolar recruitment) with $\hat{V}_0 (= A_s \cdot \hat{y}_0)$ indicating an elemental volume increase due to the piston displacement of $\hat{y}_0$. Any further change in pressure results in a volume increase as the piston moves to the right ($0 < \hat{y}_j < \hat{y}_T$) (simulating the elastic distension of the alveolar wall tissues) until it reaches the end of the cylinder ($\hat{y}_j = \hat{y}_T$) as a state of fully-distended element (Fig. 1(b) shows an alveolar element during deflation.). An application of the Boltzmann statistical model, which assumes that there is no limit in the number of alveolar elements per energy state, yields a normal (bell-shaped) distribution as the most probable distribution of alveolar elements over P_{cj}, dN_j/N (= a number fraction of elements, for which the magnitude of P_{cj} ranges between P_{cj} and $P_{cj} + dP_{cj}$)

$$\frac{dN_j}{N \cdot dP_{cj}} = f(P) \quad \text{with} \quad f(P) = \frac{\Lambda}{4P_0} \cdot exp\left(-\left(\frac{\sqrt{\pi}}{4}\Lambda\right)^2\left[\frac{P_{cj} - (P - P_0)}{P_0}\right]^2\right) \tag{2}$$

In a given pressure P, the mean distribution is $P - P_0$ with the standard deviation $\sigma_D = (8/\pi)^{\frac{1}{2}} P_0 / \Lambda \approx 1.596 \cdot P_0/\Lambda$. Thus, P_0 controls the mean (the higher P_0, the lower mean) and Λ controls the standard deviation (the higher Λ, the lower standard deviation) of the normal probability distribution function over the alveolar openings pressure (P_{cj}).

Expressed in terms of non-dimensional volume ($\overline{V}$) and non-dimensional pressure ($\overline{P}$), are [5].

$$\overline{V} = erf\left(\frac{\sqrt{\pi}}{4}\Lambda\overline{P}\right) \quad \text{with} \quad \overline{V} = \frac{V - (V_U - \Delta V/2)}{\Delta V/2}, \quad \overline{P} = \frac{P}{P_0} - 1 \tag{3}$$

$$\frac{dN_j}{N \cdot d\hat{P}_{cj}} = F(\overline{P}) \quad \text{with} \quad F(\overline{P}) = \frac{\Lambda}{4} \cdot exp\left(-\left(\frac{\sqrt{\pi}}{4}\Lambda\right)^2[\hat{P}_{cj} - \overline{P}]^2\right) \tag{4}$$

where $\hat{P}_{cj} = P_{cj}/P_0$ with the standard deviation, $\sigma = (8/\pi)^{\frac{1}{2}}/\Lambda$. It should be noted that both the normalized P-V equation and the normalized distribution depend on the magnitude of a single non-dimensional parameter, Λ. Fig. 1(e) sketches the non-dimensional normal distribution, Eq. (4), at $P = P_0$ for selected patients with ARDS and a healthy human.

By summing (integrating) the volume of each element over all open elements, the model yields two P-V equations, one for the low-P region and the other for the high-P region [6]. The equation for the high-P region is the error function P-V equation (= Eq. (1)). However, Eq. (1) with the four adjusting parameters had been shown to be an excellent

Table 1
Inflation P-V curve parameters of DG1 and DG2.

		Λ	P_0 [cmH_2O]	ΔV [L]	V_L [L]	$\hat{y}_{T0}$	P_{ID} [cmH_2O]
DG1	Bef.Inj.	1.25	12.57	1.12	−0.24	0.22	32
	Aft.Inj.	2.96	20.79	0.86	−0.03	0.84	32
DG2	Control	1.10	8.36	1.50	−0.34	0.10	30
	Aft.Inj.	5.40	22.29	1.12	−0.02	0.76	35

Table 2
Inflation Parameters of DG3. ARDS patients.

Data	Λ	P_0 [cmH_2O]	ΔV [L]	V_L [L]	$\hat{y}_{T0}$
A	2.96	22.40	2.37	−0.07	0.347
D	1.63	13.32	3.16	−0.57	0.379
G	1.73	20.16	3.10	−0.36	0.447
J	2.79	26.21	3.73	−0.16	0.474
K	2.43	17.89	1.34	−0.10	0.440
L	1.25	11.59	1.25	−0.28	0.695
O	1.95	18.37	1.88	−0.24	0.389
R	1.17	13.99	2.07	−0.51	0.406
T	5.47	30.04	1.77	−0.01	0.289

Table 3
Inflation Parameters of DG4. ARDS patients.

Data	Λ	P_0 [cmH_2O]	ΔV [L]	V_L [L]	$\hat{y}_{T0}$
6	4.14	21.60	1.07	−0.03	0.60
9	4.92	27.82	1.14	−0.01	0.55
11	1.73	18.45	3.86	−0.56	0.59
24	2.69	20.53	1.47	−0.06	0.93
30	3.40	22.18	2.87	−0.04	0.54
32	2.00	18.07	1.72	−0.22	0.73

approximation for both inflation- and deflation- P-V curves over the entire P-region [5,7].

2.2. Data groups

Five data groups, all from a previously published data sets [42] was used for the analyses in this report. These datasets were obtained by procedures that satisfied the animal care and use requirements of respective institution. The description of these data groups are as follows:

(1) Data group 1 [53]: Canine model of acute lung injury before (Data group 1 Before Injury) and after oleic-acid-induced injury (Data group 1 After Injury)
(2) Data group 2 [23]: Canine model of acute lung injury by saline lavage; Control (Data group 2 Before Injury) vs. after lung injury (Data group2 After Injury),
(3) Data group 3 [67]: P-V curves of patients with ARDS,
(4) Data group 4 [1, 2, 3]: P-V curves of patients with ARDS,
(5) Data group 5 [52,55]: P-V curves of healthy humans.

Tables 1–4 list parameters of the inflation P-V curves and Tables 5–7 list parameters of the deflation P-V curves of Data group 1 through Data group 4. Selected P-V inflation curves are shown in Fig. 2.

Table 4
Inflation Parameters of DG4. ARDS patients.

Data	Λ	P_0 [cmH_2O]	ΔV [L]	V_L [L]
ec	1.34	13.47	6.40	−2.06
gf	1.05	6.44	6.52	−1.66
hh	1.23	11.04	5.10	−2.12
jk	1.15	9.41	6.24	−1.47
rt	1.10	7.95	5.35	−1.31

Data from Ref. [23].

Table 5
Deflation P-V Curve Parameters of Data group 1, Data group 2.

		Λ^d	P_0^d [cmH_2O]	ΔV^d [L]	V_L^d [L]
Data group 1	Bef.Inj.	0.28	2.0	1.43	−0.40
	Aft.Inj.	0.40	3.8	1.11	−0.33
Data group 2	Bef.Inj.	0.22	1.3	2.02	−0.90
	Aft.Inj.	1.45	9.8	1.19	−0.14

Table 6
Deflation Parameters of Data group 3 ARDS patients.

Data No	Λ^d	P_0^d [cmH_2O]	ΔV^d [L]	V_L^d [L]
A	1.47	11.41	1.92	−0.15
D	1.08	6.85	2.70	−0.61
G	0.98	8.14	1.28	0.05
J	1.66	13.40	1.89	0.03
K	1.06	9.78	1.51	−0.37
L	0.31	3.15	1.39	−0.81
O	1.06	10.97	1.87	−0.32
R	0.86	8.14	1.83	−0.49
T	4.51	23.62	1.17	0.11

Table 7
Deflation Parameters of Data group 4. ARDS patients.

Data	Λ^d	P_0^d [cmH_2O]	ΔV^d [L]	V_L^d [L]
6	2.38	14.71	1.09	−0.06
9	5.64	21.77	0.90	−0.25
11	0.98	12.03	2.40	−1.00
24	1.89	15.89	1.52	−0.14
30	2.96	14.01	2.27	−0.45
32	1.25	11.86	1.76	−0.26

2.3. ARDS stages

In Ref. [42], four stages of ARDS (Early ARDS, Deep Knee, Advanced ARDS and Baby Lung) were identified and defined in terms of parameters of inflation P-V curves (Λ and ΔV). Fig. 3, copied from Ref. [42], depicts ΔV (VLC) vs. Λ, showing the process from healthy humans (high ΔV, low Λ) to four stages of ARDS; Early ARDS (reduced ΔV with a higher Λ-value, compared to data sets of healthy humans), Deep Knee (low ΔV, high Λ with very low starting compliance on the inflation P-V curve), Advanced ARDS (low ΔV, medium Λ), and Baby Lung (low ΔV, low Λ).
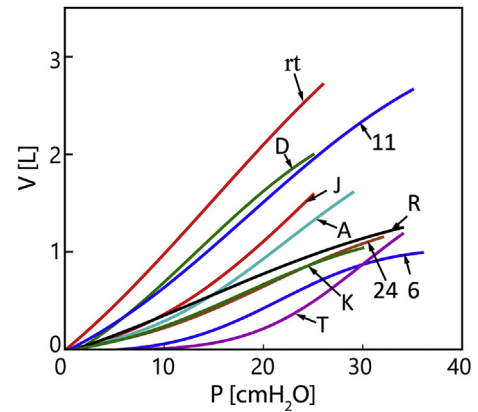
Fig. 2. P-V inflation curves selected from Data group 3 (ARDS data sets A, D, J, K, R, T), Data group 4 (ARDS data sets 6, 11, 24) and Data group 5 (healthy human data set.*rt*)
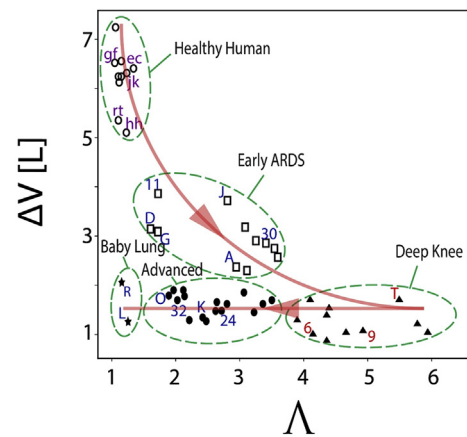
Fig. 3. ΔV vs. Λ for all data sets from Data group 3 (patients with ARDS), 4 (patients with ARDS) and 5 (healthy humans). Path from Healthy Human to Deep Knee via Early ARDS is characterized by decreasing ΔV and increasing Λ; while, path from Deep Knee to Baby Lung via Advanced ARDS is marked by a decreasing order of magnitude of Λ with ΔV limited to a narrow range.

3. Methods of analyses

In this section, we first presented the two basic mechanical ventilation strategies. One which is initiated from the inflation limb of the P-V curve or called inflation from FRC (IFRC) and the other which is initiated from the deflation limb or called deflation from TLC (DTLC). All other mechanical ventilation strategies can be seen as some combinations of these two basic strategies [23]. Next, based on the respiratory system model, we provided our quantitative derivation of the tidal recruited volume and tidal hyperinflated volume as functions of PEEP and Tidal Pressure for each type of mechanical ventilation strategies (IFRC or DTLC).

3.1. Tidal loop analyses: IFRC vs. DTLC

The mechanical ventilation strategy must be optimized by taking into account the degree of severity in ARDS. Analyses were made on cyclic inflation-deflation loops (to be referred to as tidal loops, simulating mechanical ventilation) between a high pressure (Peak) and a low pressure (PEEP (ZEEP) = positive (zero) end-expiratory pressure)
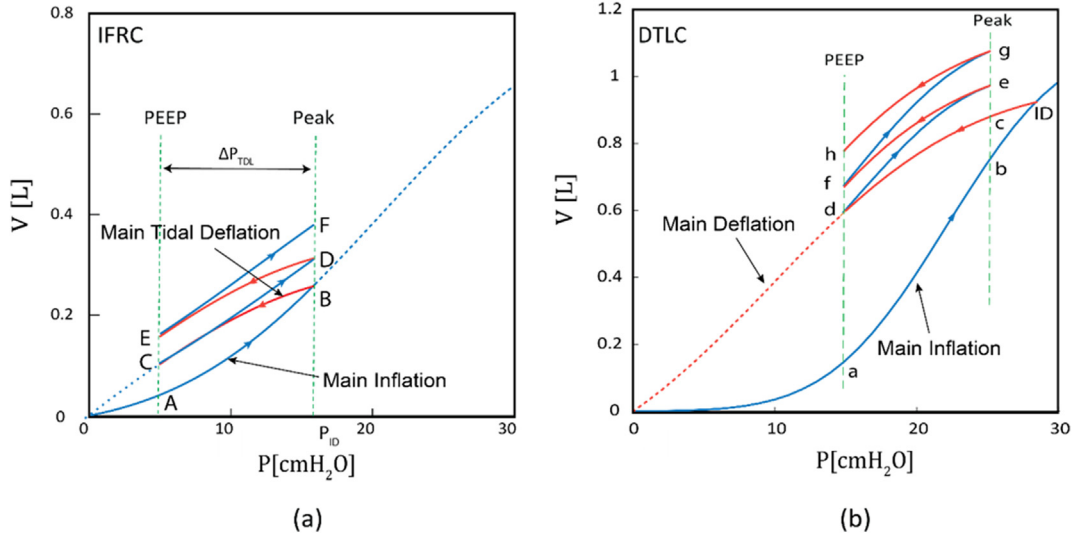
Fig. 4. Two modes of tidal loop analyzed: (a) IFRC (Tidal loop after Inflation from Functional Residual Capacity), (b) DTLC (Tidal loop after Deflation from Total Lung Capacity).

along a specified envelope P-V curve of inflation and deflation. There are two basic modes of small-volume tidal loop for mechanical ventilation in relation to the main (inflation and deflation) P-V curves [23]. They are,

(1) Tidal loop performed after Inflation from FRC (IFRC),
(2) Tidal loop performed after Deflation from TLC (DTLC).

The two modes are sketched in Fig. 4(a) and (b).

In IFRC (Fig. 4(a)), after inflation from P = 0 to a certain (tidal) peak pressure, the tidal loop begins with a main tidal deflation limb (MTD) followed by a tidal inflation limb and then a tidal deflation limb over the tidal pressure of ΔP_{TDL} = Peak - PEEP.

In DTLC (Fig. 4(b)), on the other hand, after deflation from a certain high pressure, P_{ID}, preceded by a main inflation process, the first tidal loop is initiated as a tidal inflation, followed by a tidal deflation; therefore, in Fig. 4(b), the path from P = 0 to a fully-developed tidal loop may be expressed as [*Path* O (Origin) → a→ b→ ID] = main inflation, [*Path* ID → c→ d] = main deflation, [*Path* d→ e] = tidal inflation 1, [*Path* e→ f] = tidal deflation 1, [*Path* f→ g] = tidal inflation 2, [*Path* g→ h] = tidal deflation 2.

Based on the parameters of the main inflation and the main deflation, quantitative analyses may be made on the recruitment due to tidal loops for the case of DTLC. For IFRC, on the other hand, it is necessary to estimate the four parameters, defined as $\Lambda^d_{MTD}, P^d_{0\,MTD}, V^d_{U,\,MTD}, \Delta V^d_{MTD}$ of the main tidal deflation corresponding to the process $B \to C$ in Fig. 4(a) when Peak is varied between Peak = ΔP_{TDL} (i.e. the case of ZEEP) and Peak = P_{ID}. These four parameters are estimated from the following four relations: (1) $\Lambda^d_{MTD} = \Lambda^d$, (2) $V^d_{MTD}(P = Peak) = V(P = Peak)$ (volume equality between the main inflation and the main tidal deflation at $P = Peak$) (3) $V^d_{U,\,MTD}$ in terms of the inflation parameters, (4) $V^d_{MTD}(P = 0)$ = specified (zero for the case of no airway closure during the main tidal deflation). The first relation implies that, for a specified respiratory system, the normalized distribution is similar in shape for all main tidal deflation curves.

3.2. Analyses of mechanical ventilation

3.2.1. Derivation of tidal recruited volume

According to the respiratory system model, the P-V curve of the inflation (deflation) process is related to the distribution of the alveolar elements over their opening (closing) pressure (Eq. (2)). A theoretical prediction of tidal recruited- or derecruited-volume in a tidal pressure loop may be made from the distribution of elements over the alveolar opening/closing pressure (P_{cj}/P^d_{cj}). P_{cj} of inflation and P^d_{cj} of deflation are independent of each other as random variables of the inflation- and the deflation-distribution [6]. Hence, the number fraction of alveolar elements that are recruited during the inflation from P_i to P_e, and subsequently derecruited during the deflation from P^d_i to P^d_e may be expressed in a joint distribution represented by a product of the inflation and the deflation distribution function. (See Appendix for derivation of equations presented below.)

3.2.1.1. Case IFRC. For IFRC (tidal loop after inflation from FRC) sketched in Fig. 4(a),

$V_{rec.IFRC} \equiv$ (volume recruited in IFRC between PEEP and Peak)

$$= \frac{\Delta V}{4(1 + \hat{y}_{T0})} \cdot K_3 \cdot \frac{\Delta V^d_{MTD}}{\Delta V} K^d_{3MTD} \tag{5}$$

where $K_3 = I_3(Peak) - I_3(PEEP)$, $K^d_{3\,MTD} = (I^d_{3,MTD}(Peak) - I^d_{3,MTD}(PEEP))$, $\hat{V}_0\,N =$ the total volume available for recruitment, $I_3(P) = erf\,(C(P/P_0 - 1))$, $I^d_{3\,MTD}(P) = erf\,(C^d(P/P^d_{0\,MTD} - 1))$, $C = \sqrt{\pi}\,\Lambda/4$, $C^d = \sqrt{\pi}\,\Lambda^d/4$.

3.2.1.2. Case DTLC. For DTLC (tidal loop after deflation from TLC) sketched in Fig. 4(b),

$V_{rec.DTLC} \equiv$ (volume recruited in DTLC between PEEP and Peak)

$$= \frac{\Delta V}{4(1 + \hat{y}_{T0})} \cdot K_3 \left[1 - \frac{I^d_3(P_{ID}) - I^d_3(Peak)}{I^d_3(P_{ID}) - I^d_3(PEEP)} \right] \cdot \frac{\Delta V^d}{\Delta V} K^d_3 \tag{6}$$

where $K^d_3 = (I^d_3(Peak) - I^d_3(PEEP))$, $I^d_3(P) = erf\,(C^d(P/P^d_0 - 1))$.

There have been many, sometimes conflicting, reports on the optimization of mechanical ventilation such as (1) high PEEP for high recruitment [10,21,45], (2) low tidal volume for protection against ventilator-induced lung injury (VILI) [43], (3) high PEEP as cause of VILI [4,24,29,50,51]. Here, as an indicator of VILI, we proposed equations for the total volume of elements which are open and fully distended during the mechanical ventilation between PEEP and Peak.

3.2.2. Derivation of tidal hyperinflation

Tidal Hyperinflated volume is the total volume of alveolar elements that are fully-distended throughout the tidal cycles. Here, we provided its derivation for both cases of IFRC and TDLC.

3.2.2.1. Case IFRC. For IFRC (Fig. 4(a)), It had been shown that alveolar elements with $P_{cj} = 0$ (= elements which pop open at P = 0 (Fig. 1(a)) are fully distended (i.e. the piston reaches its stroke limit of $\hat{y}_T$ in our model of an element (Fig. 1(a)) at $P = P_0 \cdot \hat{y}_{T0}$ [6]. Therefore, at $P = Peak$ along the main inflation (Location B in Fig. 4(a)), elements with $0 \leq P_{cj} \leq Peak - P_0 \cdot \hat{y}_{T0}$ are exposed to pressure higher than the pressure for full distension (to be referred to as the state of hyperinflation). A similar argument on MTD (deflation limb of B → C → O in Fig. 4(a)) indicates that elements with $P_{cj}^d = PEEP - P_0^d \hat{y}_{T0}^d$ begin the contraction at PEEP (= Location C in Fig. 4(a)). However, $P_0^d \hat{y}_{T0}^d$ is very small (below 1 $[cmH_2O]$) compared to $P_0 \hat{y}_{T0}$ of 5–20 $[cmH_2O]$ for patients with ARDS [7]; hence, we postulated that the elements with $0 \leq P_{cj}^d \leq PEEP$ in Fig. 4(a) remain at the state of overdistension.

With the number fraction (NF) defined as a number of alveolar elements as a fraction of the total number of elements, let NF_{HI} = Number fraction of elements exposed to pressure higher than the pressure needed for the state of full distension of $P_{cj} + P_0 \hat{y}_{T0}$, and noting $N\hat{V}_{distension}$ (= total volume available for distension against the spring of the alveolar element in the model) $= \Delta V \cdot (\hat{y}_{T0}/(1 + \hat{y}_{T0}))$, the following equations have been developed;

Case 1. $Peak (=P_{ID}) < P_0 \hat{y}_{T0}$

$V_{HI\ IFRC} Total$ (= volume of elements undergoing over-distension) = 0.

Case 2. $Peak (=P_{ID}) \geq P_0 \hat{y}_{T0}$

$V_{HI\ IFRC} Total = V_{HI\ IFRC}1 + V_{HI\ IFRC}2$
$$V_{HI\ IFRC}1 = \Delta V (\hat{y}_{T0}/(1 + \hat{y}_{T0})) \cdot NF_{HI\ IFRC}1 \tag{7}$$

where $V_{HI\ IFRC}1$ = total volume of fully-distended elements that are exposed to a pressure level higher than the pressure required for full-distension throughout the tidal cycles of IFRC with $NF_{HI\ IFRC}1$ defined as

$$\frac{1}{2}(I_3(Peak - P_0\hat{y}_{T0}) + I_1) \cdot \frac{\Delta V_{MTD}^d}{\Delta V} \cdot \frac{1}{2}(I_{3\ MTD}^d(PEEP) + I_{1\ MTD}^d)$$

= NF of elements, fully-distended at the initial main inflation → MTD stage of 0 → B → C in Fig. 4(a), and remain fully-distended throughout the tidal ventilation between PEEP and Peak where $I_1 = erf(C)$, $I_{3\ MTD}^d = erf(C^d) (=I_1^d)$.

$V_{HI\ IFRC}2 = 0$ if $\Delta P_{TDL} < P_0 \hat{y}_{T0}$

$V_{HI\ IFRC}2 = \Delta V (\hat{y}_{T0}/(1 + \hat{y}_{T0})) \cdot NF_{HI\ IFRC}2$ if $\Delta P_{TDL} \geq P_0 \hat{y}_{T0}$ where $NF_{HI\ IFRC}2 = \frac{1}{4}(I_3(PEEP + P_0\hat{y}_{T0}) - I_3(PEEP)) \frac{\Delta V_{MTD}^d}{\Delta V} K_{3\ MTD}^d$ = number fraction of elements, which go through the cycle of pop-open → fully-distended → pop-close during the ventilation between PEEP and Peak.

3.2.2.2. Case DTLC. For DTLC (Fig. 4(b)), with similar approach:

Case 1. $P_{ID} < P_0 \hat{y}_{T0}$

$V_{HI\ DTLC} Total = 0.$

Case 2. $P_{ID} \geq P_0 \hat{y}_{T0}$

$V_{HI\ DTLC} Total = V_{HI\ DTLC}1 + V_{HI\ DTLC}2.$
$$V_{HI\ DTLC}1 = \Delta V (\hat{y}_{T0}/(1 + \hat{y}_{T0})) \cdot NF_{HI\ DTLC}1 \tag{8}$$

where $NF_{HI\ DTLC}1 = \frac{1}{4}(I_3(P_{ID} - P_0\hat{y}_{T0}) + I_1) \cdot (\Delta V^d/\Delta V) \cdot (I_3^d(PEEP) + I_1^d)$. = number fraction of elements fully-distended in the main inflation, $0 \to a \to ID$ in Fig. 4(b), and stay fully-distended since their closing pressure lies between d (= PEEP) and 0 (Origin). $V_{HI\ DTLC}2 = 0$ if $\Delta P_{TDL} < P_0\hat{y}_{T0}$, $V_{HI\ DTLC}2 = \Delta V (\hat{y}_{T0}/(1 + \hat{y}_{T0})) \cdot NF_{HI\ DTLC}2$ if $\Delta P_{TDL} \geq P_0 \hat{y}_{T0}$ where. $NF_{HI\ DTLC}2 = \frac{1}{4}(I_3(PEEP + P_0\hat{y}_{T0}) - I_3(PEEP)) \frac{\Delta V^d}{\Delta V} K_3^d$

4. Results

We first attempted to evaluate our analytical predictions of tidal recruited volume by comparing them to a similar experimental work being found in the literature [23]. We then presented our quantitative prediction of tidal recruited volume and tidal hyperinflated volume as functions of PEEP and tidal pressure by using quasi-static P-V curves of human subjects in healthy and various ARDS conditions.

4.1. Experiments vs. theory

In an experimental study [23], the total volume increase from six canine models as a function of PEEP is measured and shown (dotted curves) in Fig. 5 as top graphs; These experiments were done in cases of IFRC in Fig. 5(a) and DTLC in Fig. 5(b). For each case of IFRC and DTLC, the left and right graphs is for the uninjured and injured canine models respectively. The bottom graphs in both Fig. 5(a) and (b) are our
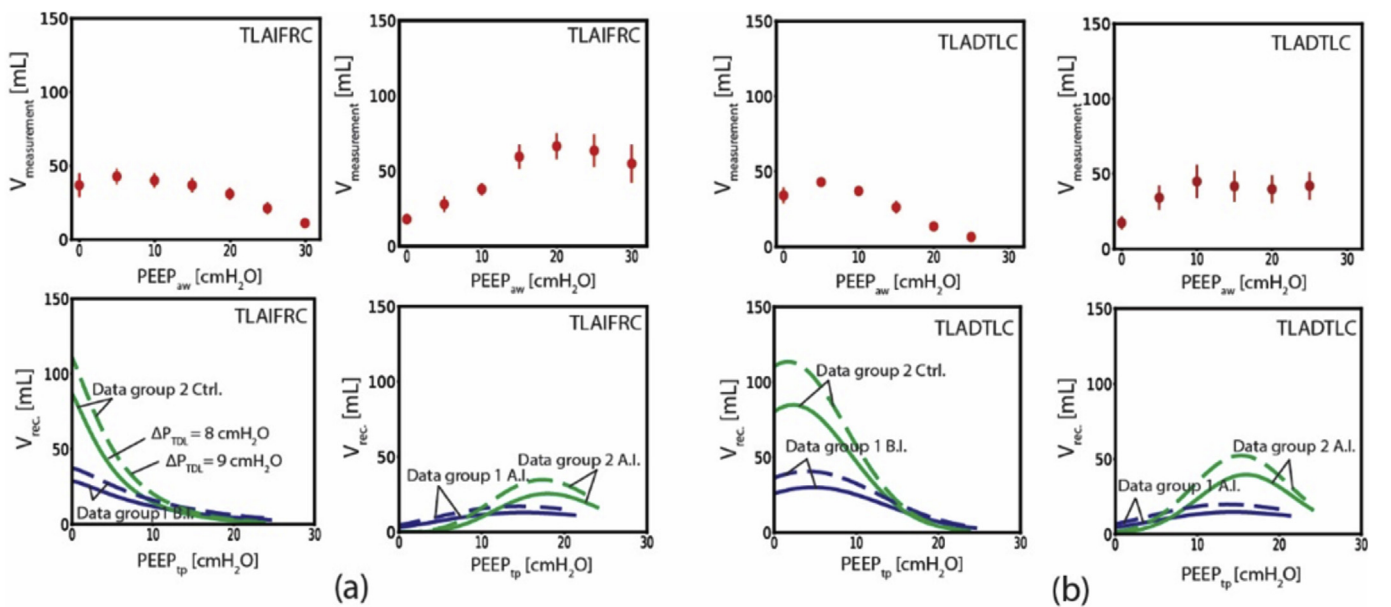
Fig. 5. Experiments vs. Theory on $V_{rec.} - PEEP$. (a) IFRC, (b) DTLC. Top dotted curves = measurements by Ref. [23] at $\Delta P_{aw} = 10[cmH_2O]$, PEEP in airway pressure, Bottom curves = theoretical predictions for canine ARDS models of Data group 1 and Data group 2 for $\Delta P_{tp} = 8 [cmH_2O]$ (solid), 9 $[cmH_2O]$ (dotted). PEEP in transpulmonary pressure, Left-hand side = Before Injury, Data group 1 and Data group 2. Right-hand side = After Injury, Data group 1 and Data group 2.
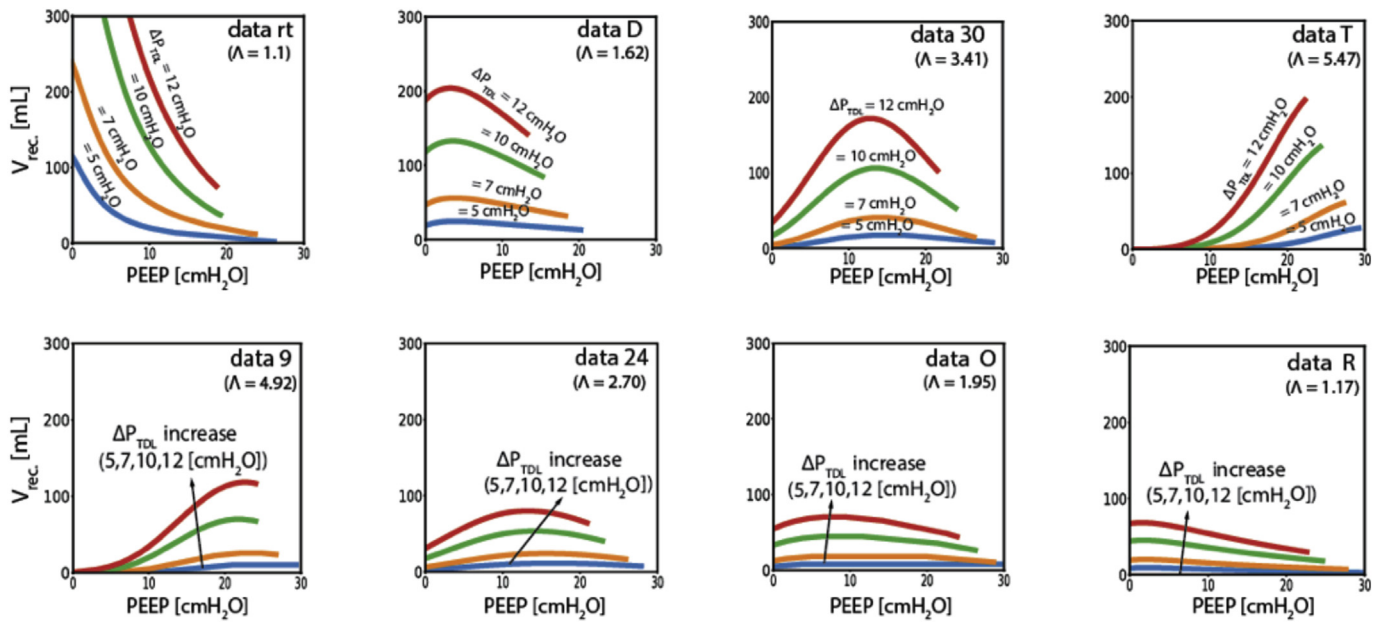
Fig. 6. $V_{rec.}$ vs. PEEP at ΔP_{TDL} = 5, 7, 10, 12 [cmH_2O] for IFRC. Data set: rt = Healthy Human, D and 30 = Early ARDS, T and 9 = Deep Knee, 24 and O = Advanced ARDS, R = Baby Lung. Our computational results show a degree of PEEP for maximum recruited volume shifting to a higher level from Healthy Human to Deep Knee; then, decreasing to Baby Lung via Advanced ARDS.

model predictions for Before Injury and After Injury (Data group 1 and 2) on the left and right respectively. As described in Ref. [5], the transpulmonary pressure (= P_{tp}), which is the pressure used in our recruitment analysis, is less than the corresponding airway pressure by 10–20%. Therefore, for better comparison with the experimental results, $V_{rec.}$ vs. PEEP relation of our predictions (Eq. (5) for IFRC, Eq. (6) for DTLC) are shown in Fig. 5 as bottom graphs when ΔP_{TDL} is set to 8.0 [cmH_2O] (dotted) and 9.0 [cmH_2O] (solid) in transpulmonary pressure (**tp**).

This experimental study, was the only experimental work on the literature we were able to find that measured respiratory volume increase as functions of PEEP in the conditions of IFRC and DTLC. However, there still exists some differences between the conditions of this experimental work and our analytical predictions. These differences are as follows: 1) The experimental measurements yield the total volume increase (by pop-open mechanism as well as by alveolar distension) under the dynamic conditions; while, our theoretical predictions are the volume recruited by the pop-open mechanism only, based on the quasi-static P-V curve. 2) The canine subjects of the experimental work are different than the canine subjects we used in our analytical work. 3) The reported measurements in the experimental work are the mean and standard deviation of the measurements of the six canine subjects, whereas we reported our predictions on individual subjects separately. 4) Finally, ΔP_{TDL} (= Peak - PEEP) of these experimental measurements was 10 [cmH_2O] in airway pressure (**aw**). However, in our prediction, the ΔP_{TDL} is in transpulmonary pressure (**tp**) as the quasi-static P-V curves are usually measured in transpulmonary pressure.

Considering these differences, our quantitative predictions are in satisfactory agreement with the experimental results. The tidal recruited volume function predicted from the present analyses are in the same order of magnitude and similar in variations as the measurement results. Moreover, both experimental and our prediction results similarly suggest that PEEP value required to achieve maximum volume recruitment is very low for healthy subjects (left) and is relatively high for the injured group (right) for both cases of IFRC (a) and DTLC (b).

4.2. Prediction of tidal recruited volume and hyperinflated volume among ARDS patients

The mechanics of the respiratory system is subject to significant changes as the degree of severity of ARDS advances. This leads the optimum PEEP and Tidal Pressure to be changed based on the severity of ARDS. Among the fifty P-V curves of Healthy and ARDS subjects provided in the work [17], we randomly picked one healthy human (Data R), two subjects with Early ARDS characteristics (Data D and 30), two subjects with Deep Knee ARDS (Data T and 9), two Advanced ARDS (Data 24 and O) and one Baby Lung ARDS (Data R). We therefore, for the rest of the work made similar predictions and visualization of recruited volume and overdistension for all these eight subjects based on their quasi-static pressure volume curve.

In Fig. 6, using equation (5), we illustrated the tidal recruited volume as a function of PEEP and tidal pressure in the case of IFRC for all the eight subjects from Healthy Human (Data rt) to Baby Lung (Data R). Similarly, in Fig. 7, based on equation (6), tidal recruited volume is plotted for the case of DTLC. In Fig. 8, we simultaneously plotted volume recruitment for the case of IFRC and DTLC for the purpose of comparison. As illustrated in Fig. 9, we used equation (7), to predict the hyperinflation as functions of PEEP and tidal pressure in the case of DTLC for all the eight subjects. Finally, for the purpose of optimization of mechanical ventilation, we simultaneously showed our prediction of recruitment volume and hyperinflation for the case of DTLC as function of PEEP with the tidal pressure = 10[cmH_2O].

5. Discussion

Current ventilation strategies include low tidal volumes of 6 mL per kilogram of predicted body weight [44] as "one-size-fits-all" for ARDS patients with the PEEP being chosen in the range of 0–10 cmH_2O adjusted in reaction to changes in oxygenation [8,11]. Many physicians do not strictly stay with the 6 mL per kilogram for tidal volume. Moreover, there are evidences that optimizing PEEP based on the oxygenation shown not to correlate well with pathologic changes in lung mechanics and may cause ventilator-induced lung injury (VILI) [11,68].
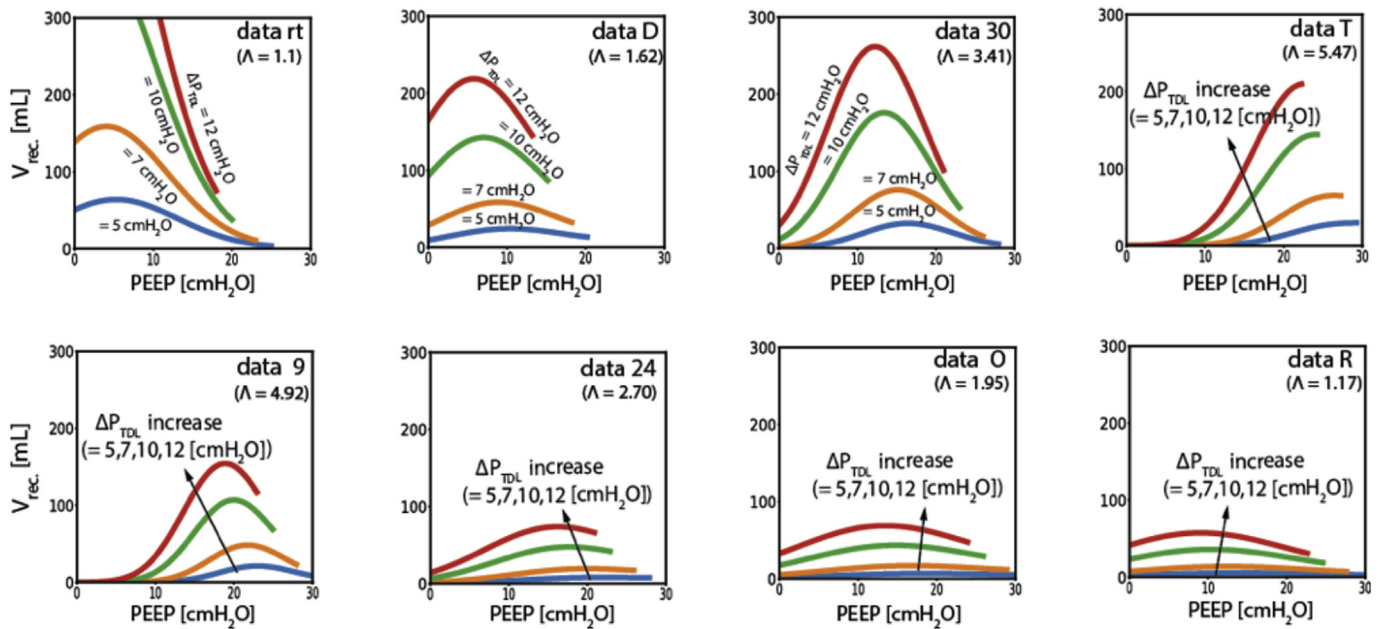
Fig. 7. $V_{rec.}$ vs. PEEP at ΔP_{TDL} = 5, 7, 10, 12 [cmH_2O] for DTLC. Data sets same as Fig. 6. Differences between IFRC (Fig. 6) and DTLC reflect the path-dependency of the ventilation.

In this paper, we combined our respiratory system model with the patient-specific quasi-static P-V data of ARDS patients to analytically predict the effects of tidal pressure (volume) and PEEP on the recruitment and hyperinflation of individual ARDS patients.

According to the respiratory system model (as described in the background section), two model parameters P_0 and Λ are respectively determining the mean and the standard deviation of the alveolar pop-open pressure distribution function described in Eq. (2). An increase in P_0 yields decrease in mean and similarly, increase in Λ results in the decrease in the standard deviation of the distribution function.

Therefore, based on the values for the P_0 and Λ being determined from each subject's P-V curve, the variations in the shape of the alveolar pop-open distribution function between ARDS stages is observed as follows:

Starting with the Healthy human group, the mean and the standard deviation of the alveolar opening pressure are very large (since P_0 and Λ are very low, see Eq. (2)). However, in the Early ARDS groups, the mean and the standard deviation significantly decreases until the Deep Knee stage in which the mean and the standard deviation reaches to the lowest values, thus forming a sharp distribution function for the alveolar opening pressure. With further advancement in the degree of
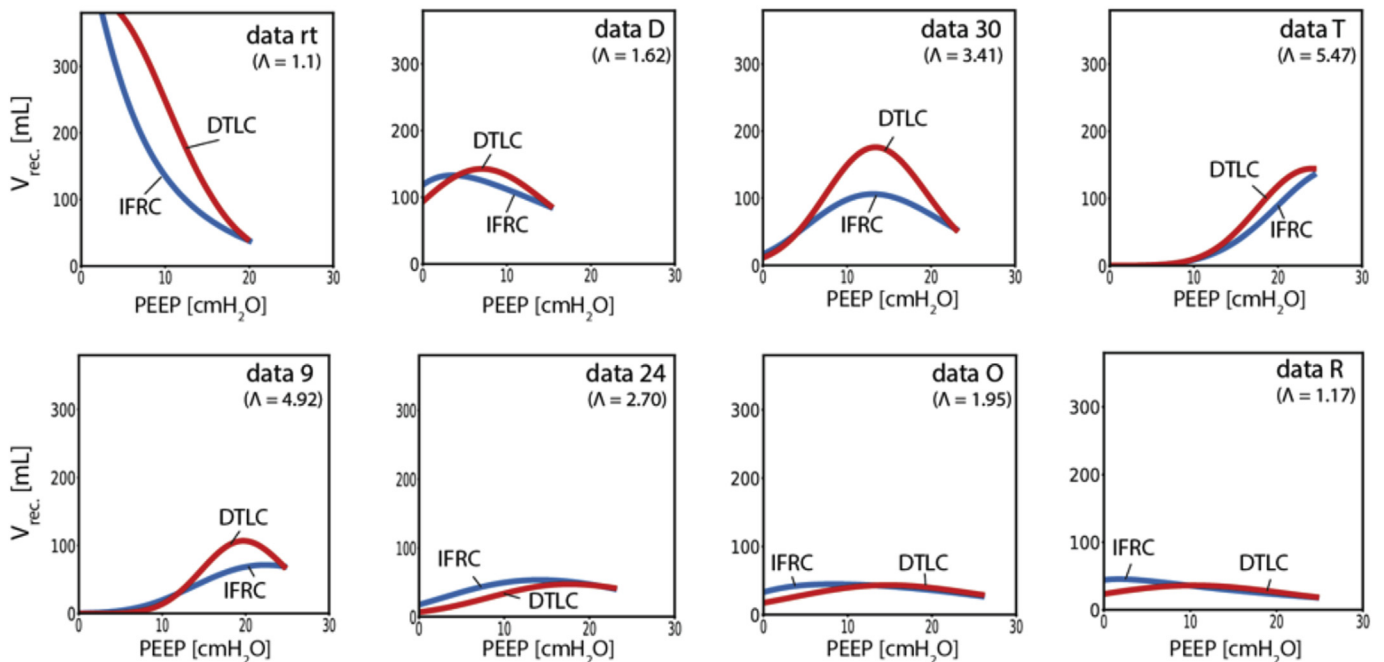

Fig. 8. $V_{rec.}$ vs. PEEP. Comparison between DTLC and IFRC at ΔP_{TDL} = 10 [cmH_2O]. Data sets same as Fig. 6. Maximum recruited volume is achieved by DTLC for Early ARDS and Deep Knee; while, IFRC yields a slightly higher recruited volume for Advanced ARDS and Baby Lung.

Fig. 9. V_{rec}. vs. PEEP. Comparison between DTLC and IFRC at $\Delta P_{TDL} = 10 \, [cmH_2O]$. Data sets same as Fig. 6. Maximum recruited volume is achieved by DTLC for Early ARDS and Deep Knee; while, IFRC yields a slightly higher recruited volume for Advanced ARDS and Baby Lung.
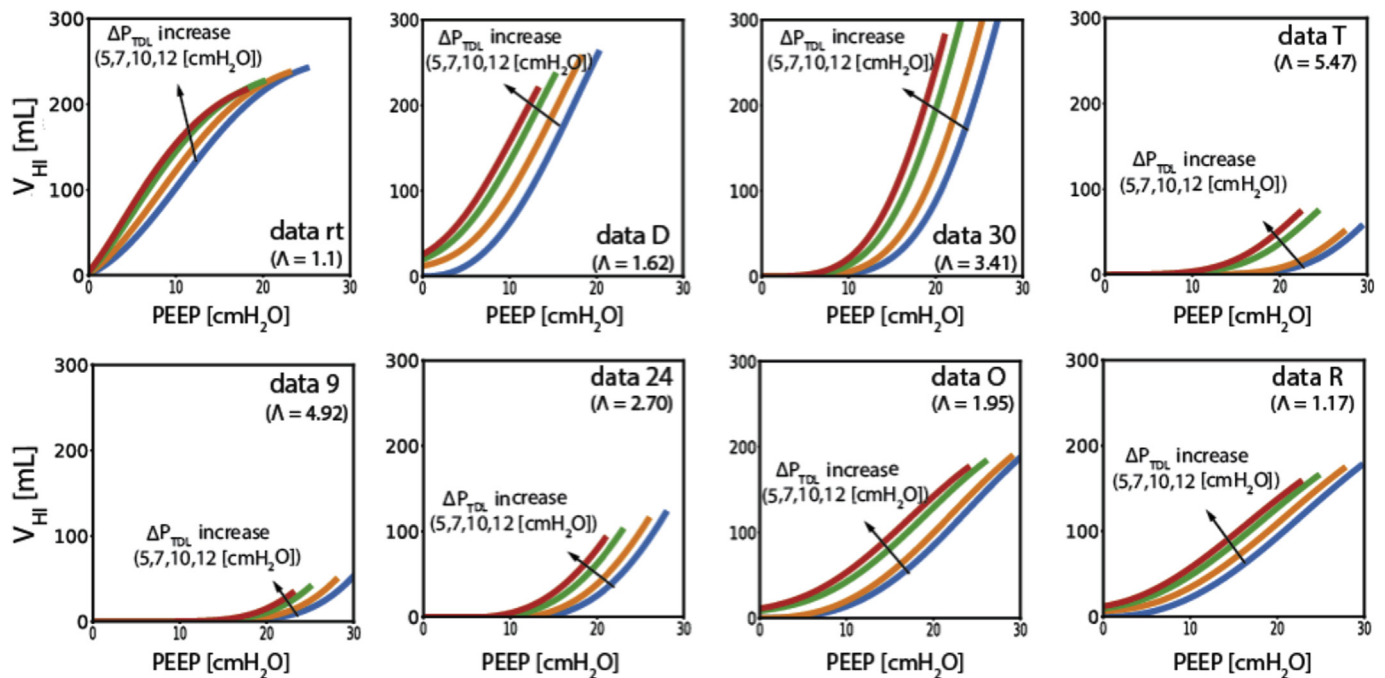
severity of ARDS, an opposite trend is observed as the mean and standard deviation are starting to increase within the Advanced ARDS group up to the Baby-Lung ARDS group where the mean and the standard deviation reaches to the highest values and almost equal to the values in the Healthy Lung group. This is due to the fact that the healthy human group and Baby-Lung ARDS group have similar distribution function of the alveolar pop-open pressure. However, it is noted that according to Fig. 6, vital lung capacity (ΔV) in healthy human group is about 5–7 times larger than the Baby Lung groups. These quantitative findings are in agreement with the concept of Baby-Lung which originates from the observation through the computed tomography of ALI/ARDS patients that the normal state of their respiratory system has the properties of a healthy human but the dimension of that of small children [30]. This suggests that the total respiratory system of ARDS patients with "baby lung" may be small, but similar in mechanics to that of the healthy humans.

Our model predictions of the tidal recruited volume for the case of IFRC (see Fig. 6) suggest that PEEP = 0 (natural breathing [64]) yields the maximum recruitment for Healthy Human (Data rt). Healthy human respiratory system during one cycle of quiet natural breathing (which always taking place at PEEP = 0), creates up to $6 cmH_2O$ transpulmonary pressure and the volume of $500 mL$ [16]. Our model predicts (see Fig. 6, data rt at PEEP = 0) that $150 - 200 mL$ of this volume yields to the recruited volume. In the Early ARDS, the decrease in the mean and standard deviation of the distribution of alveolar elements over the pop-open pressure resulted in the location of the maximum of tidal recruited volume shifting away from ZEEP to a higher level of PEEP. As the degree of severity of ARDS is further advancing to Deep-Knee cases (Data T and 9), the mean and the standard deviation of the pop-open distribution of the elements moves to higher values and thus our prediction suggests that the location of the maximum of tidal recruited volume shifting to the very high PEEP level. A similar continuous trend but in the opposite direction is observed for the ARDS cases of higher severity than Deep Knee. In Advanced ARDS (Data 24 and O), the PEEP corresponding to the maximum tidal recruited volume gradually returns to the lower values. This reverse behavior continues such that in the terminal stages of ARDS (Baby Lungs, Data R), the PEEP

corresponding to the maximum tidal recruited volume approaches to zero, similar to the case of a healthy lung.

Our model prediction (Fig. 6) also suggest that the Tidal recruited volume continuously and consistently decreases from the case of Healthy Lungs (Data rt) to the Baby Lungs (Data R). These predictions are consistent with many experimental measurements [25,26] which suggest the reduction of PaO_2/FiO_2 from above $500 \, mmHg$ for Healthy Lung to $201–300 \, mmHg$ for early ARDS, $101–200 \, mmHg$ for moderate ARDS and less than $100 \, mmHg$ for severe cases of ARDS.

The tidal recruited volume vs. PEEP for the case of DTLC ventilation illustrated in Fig. 7 was more or less similar to the case of IFRC in terms of the location of the optimum PEEP for each ARDS group. However, as shown in Fig. 8, DTLC case leads to higher recruited volume for the cases of healthy human, Early ARDS, and Deep Knee. As for the cases of Advanced ARDS and Baby Lung there were no significant differences observed between IFRC and DTLC.

Depicted in Fig. 9 is the tidal hyperinflated volume vs. PEEP at tidal pressure = 5, 7, 10 and 12 $[cmH_2O]$ for IFRC. As mentioned, the tidal hyperinflated volume is the total volume of alveolar elements exposed to a pressure level higher than the pressure required for the full distension throughout the tidal cycles. It is clearly observed from this figure that with the increase in tidal pressure, the volume recruitment increases in all subjects. From Healthy Human (data rt) to Deep Knee (data T and 9), the location of a significant rise in tidal hyperinflated volume above zero shifted gradually to a high PEEP region with the opposite decreasing tendency from the high PEEP to the low PEEP for Advanced ARDS and Baby Lung. Despite the general tendency of tidal recruited volume which has a maximum value at some degree of PEEP, the hyperinflation volume is always monotonically increasing with the increase in PEEP and tidal pressure [63].

In order to discuss both the recruitment effectiveness and the hyperinflation as an indicator of the risk of VILI, presented in Fig. 10 are simultaneous presentation of Tidal Recruited Volume vs. PEEP and Tidal Hyperinflation Volume vs. PEEP at $\Delta P_{TDL} = 10 \, [cmH_2O]$.

In the healthy human group (Data rt), PEEP = 0 is the optimum condition as it simultaneously maximizes the tidal recruited volume and minimizes the tidal hyperinflated volume. This optimized scenario
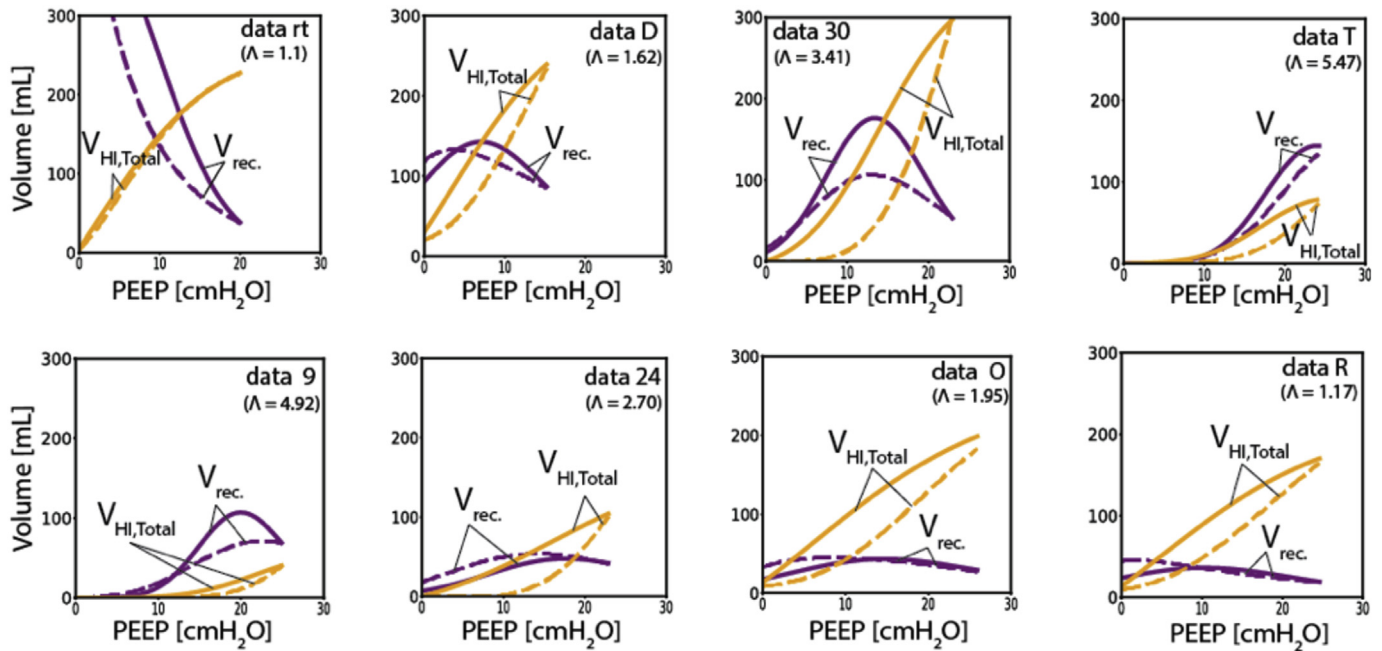
Fig. 10. $V_{rec.}$ vs. PEEP. Comparison between DTLC and IFRC at $\Delta P_{TDL} = 10$ [cmH_2O]. Data sets same as Fig. 6. Maximum recruited volume is achieved by DTLC for Early ARDS and Deep Knee; while, IFRC yields a slightly higher recruited volume for Advanced ARDS and Baby Lung.

takes place in the process of natural breathing in healthy human [64].

In cases of Early ARDS, Deep Knee ARDS and Advanced ARDS, achieving high recruited volume comes at the cost of increasing the hyperinflation. These findings are in agreement with many previous experimental observations [12,33,63]. However, in the Advanced ARDS group (data 24 and O), the recruited volume is less sensitive to the variations of PEEP while the hyperinflated volume drastically increases as PEEP is increased, suggesting a mild low PEEP to be more effective for the Advanced ARDS group.

In the case of Baby Lung ARDS (Data R), similar to Healthy Lung, PEEP = 0 simultaneously maximizes recruitment and minimizes hyperinflation. However, the tidal recruited volume in magnitude is much lower comparing to the healthy lung. According to our prediction in Fig. 6 for the Baby Lung, increasing tidal volume does not yield to significant increase in the recruited volume either. Thus, other adjunctive mechanical strategies such as partial or total extracorporeal support [28,62] maybe recommended for the Baby Lung group to compensate low recruitment volume.

Lastly, our prediction suggests that DTLC in general yields to a slightly higher recruitment while it comes at the cost of slightly higher hyperinflation comparing to IFRC.

6. Conclusion

Many previous clinical investigations pointed out needs for balancing alveolar recruitment and overdistension as well as for information on ventilation strategy more applicable to the individuals than to the population. In this work, Quasi-static P-V curves were combined with a respiratory system model (RSM) to analyze alveolar recruitment and hyperinflation during the mechanical ventilation of patients with ARDS. Using the respiratory system model, we quantified various qualitative observations reported previously. We quantitatively showed that the optimum parameters of mechanical ventilation (PEEP and Tidal Pressure) are highly dependent on the degree in the severity of ARDS. As for maximizing the recruitment, we quantitatively showed that by the advancement of the ARDS severity from Early ARDS to Deep Knee ARDS, optimum PEEP monotonically increases. However, PEEP monotonically decreases back as the severity of ARDS further advances

from Deep Knee to the terminal stages of Advanced ARDS and Baby Lung ARDS. Our quantitative predication also showed that increasing PEEP and tidal pressure will always yield to the increase in the hyperinflation with the rate of increase being varied by the degree in the severity of ARDS. Our quantitative predictions based on individuals pressure-volume curve may contribute to personalizing of mechanical ventilation of ARDS patients.

Acknowledgment

References

[1] Albaiceta Guillermo M, Luyando Luis H, Parra Diego, Menendez Rafael, Calvo Juan, Rodríguez Pedreira Paula, Taboada Francisco. Inspiratory vs. expiratory pressure-volume curves to set end-expiratory pressure in acute lung injury. Intensive Care Med 2005;31(10):1370–8.

[2] Albaiceta Guillermo M, Taboada Francisco, Parra Diego, Blanco Armando, Escudero Dolores, Otero Jesús. Differences in the deflation limb of the pressure-volume curves in acute respiratory distress syndrome from pulmonary and extrapulmonary origin. Intensive Care Med 2003;29(11):1943–9.

[3] Albaiceta Guillermo M, Taboada Francisco, Parra Diego, Luyando Luis H, Calvo Juan, Menendez Rafael, Otero Jesús. Tomographic study of the inflection points of the pressure–volume curve in acute lung injury. Am J Respir Crit Care Med 2004;170(10):1066–72.

[4] Britto Passos Amato Marcelo, Silvia Valente Barbas Carmen, Machado Medeiros Denise, Borges Magaldi Ricardo, Paula Schettino Guilherme, Lorenzi-Filho Geraldo, Adib Kairalla Ronaldo, Deheinzelin Daniel, Munoz Carlos, Oliveira Roselaine, et al. Effect of a protective-ventilation strategy on mortality in the acute respiratory distress syndrome. N Engl J Med 1998;338(6):347–54.

[5] Amini R, Barnes TA, Savran A, Narusawa U. Respiratory system model for quasi-static pulmonary pressure-volume (pv) curve: generalized pv curve analyses. J Biomech Eng 2008;130(4):044501.

[6] Amini R, Creeden K, Narusawa U. A mechanistic model for quasistatic pulmonary pressure-volume curves for inflation. J Biomech Eng 2005;127(4):619–29.

[7] Amini R, Narusawa U. Respiratory system model for quasistatic pulmonary pressure-volume (pv) curve: inflation-deflation loop analyses. J Biomech Eng 2008;130(3):031020.

[8] Andrews Penny L, Sadowitz Benjamin, Kollisch-Singule Michaela, Satalin Joshua, Roy Shreyas, Snyder Kathy, Gatto Louis A, Nieman Gary F, Habashi Nader M. Alveolar instability (atelectrauma) is not identified by arterial oxygenation

predisposing the development of an occult ventilator-induced lung injury. Intensive care medicine experimental 2015;3(1):16.

[9] Barabási Albert-László, Buldyrev Sergey V, Eugene Stanley H, Suki Béla. Avalanches in the lung: a statistical mechanical model. Phys Rev Lett 1996;76(12):2192.

[10] Sílvia Valente Barbas Carmen, Faissol Janot de Matos Gustavo, Pimentel Pincelli Mariangela, da Rosa Borges Eduardo, Antunes Telma, Monteiro de Barros Juliana, Okamoto Valdelis, Batista Borges Joao, Brito Passos Amato Marcelo, Roberto Ribeiro de Carvalho Carlos. Mechanical ventilation in acute respiratory failure: recruitment and high positive end-expiratory pressure are necessary. Curr Opin Crit Care 2005;11(1):18–28.

[11] Baumgardner James E, Markstaller Klaus, Pfeiffer Birgit, Doebrich Marcus, Otto Cynthia M. Effects of respiratory rate, plateau pressure, and positive end-expiratory pressure on pao2 oscillations after saline lavage. Am J Respir Crit Care Med 2002;166(12):1556–62.

[12] Berney Susan, Denehy Linda. A comparison of the effects of manual and ventilator hyperinflation on static lung compliance and sputum production in intubated and ventilated intensive care patients. Physiother Res Int 2002;7(2):100–8.

[13] Blankman Paul, Shono A, Hermans BJM, Wesselius T, Hasan Djo, Gommers Diederik. Detection of optimal peep for equal distribution of tidal volume by volumetric capnography and electrical impedance tomography during decreasing levels of peep in post cardiac-surgery patients. Br J Anaesth 2016;116(6):862–9.

[14] Burck Russell. Challenges of treating on the basis of knowledge: the ards network trials and the ensuing controversy. Crit Care Med 2004;32(3):904–5.

[15] Caironi Pietro, Cressoni Massimo, Chiumello Davide, Ranieri Marco, Quintel Michael, Russo Sebastiano G, Cornejo Rodrigo, Bugedo Guillermo, Carlesso Eleonora, Russo Riccarda, et al. Lung opening and closing during ventilation of acute respiratory distress syndrome. Am J Respir Crit Care Med 2010;181(6):578–86.

[16] Moran Campbell Edward James. The respiratory muscles and the mechanics of breathing. Lloyd-Luke; 1958.

[17] Caruso Pedro. Ventilator-induced lung injury distribution: the key to understanding injury mechanisms. Am J Respir Crit Care Med 2007;175(1):95a–6a.

[18] Coppola Silvia, Froio Sara, Chiumello Davide. Higher vs. lower peep in ards: just one part of the whole. J Thorac Dis 2018;10(1):56.

[19] Das Anup, Menon Prathyush P, Hardman Jonathan G, Bates Declan G. Optimization of mechanical ventilator settings for pulmonary disease states. IEEE (Inst Electr Electron Eng) Trans Biomed Eng 2013;60(6):1599–607.

[20] Dellamonica J, Lerolle N, Sargentini C, Beduneau G, Di Marco F, Mercat A, Richard JCM, Diehl JL, Mancebo J, Rouby JJ, et al. Peep-induced changes in lung volume in acute respiratory distress syndrome. two methods to estimate alveolar recruitment. Intensive Care Med 2011;37(10):1595.

[21] Di Marco Fabiano, Devaquet Jérôme, Lyazidi Aissam, Galia Fabrice, Pinto da Costa Nathalia, Fumagalli Roberto, Brochard Laurent. Positive end-expiratory pressure-induced functional recruitment in patients with acute respiratory distress syndrome. Crit Care Med 2010;38(1):127–32.

[22] DiRocco Joseph D, Carney David E, Nieman Gary F. Correlation between alveolar recruitment/derecruitment and inflection points on the pressure-volume curve. Intensive Care Med 2007;33(7):1204–11.

[23] Downie John M, Nam Arthur J, Simon Brett A. Pressure–volume curve does not predict steady-state lung volume in canine lavage lung injury. Am J Respir Crit Care Med 2004;169(8):957–62.

[24] Dueck Ron. Alveolar recruitment versus hyperinflation: a balancing act. Current Opinion in Anesthesiology 2006;19(6):650–4.

[25] Ferguson Niall D, Fan Eddy, Camporota Luigi, Antonelli Massimo, Anzueto Antonio, Beale Richard, Brochard Laurent, Brower Roy, Esteban Andrés, Gattinoni Luciano, et al. The berlin definition of ards: an expanded rationale, justification, and supplementary material. Intensive Care Med 2012;38(10):1573–82.

[26] ARDS Definition Task Force. Acute respiratory distress syndrome. Jama 2012;307(23):2526–33.

[27] Ganzert Steven, Kramer Stefan, Guttmann Josef. Predicting the lung compliance of mechanically ventilated patients via statistical modeling. Physiol Meas 2012;33(3):345.

[28] Gattinoni L, Kolobow T, Agostoni A, Damia G, Pelizzola A, Rossi GP, Langer M, Solca M, Citterio R, Pesenti A, et al. Clinical application of low frequency positive pressure ventilation with extracorporeal co 2 removal (lfppv-ecco 2r) in the treatment of adult respiratory distress syndrome (ards). Int J Artif Organs 1979;2(6):282–3.

[29] Gattinoni Luciano, Carlesso Eleonora, Brazzi Luca, Caironi Pietro. Positive end-expiratory pressure. Curr Opin Crit Care 2010;16(1):39–44.

[30] Gattinoni Luciano, Pesenti Antonio. The concept of "baby lung". Intensive Care Med 2005;31(6):776–84.

[31] Girard Timothy D, Bernard Gordon R. Mechanical ventilation in ards: a state-of-the-art review. Chest 2007;131(3):921–9.

[32] Hickling Keith G. The pressure–volume curve is greatly modified by recruitment: a mathematical model of ards lungs. Am J Respir Crit Care Med 1998;158(1):194–202.

[33] Hickling KG, Henderson SJ, Jackson R. Low mortality associated with low volume pressure limited ventilation with permissive hypercapnia in severe adult respiratory distress syndrome. Intensive Care Med 1990;16(6):372–7.

[34] Kallet Richard H, Branson Richard D. Do the nih ards clinical trials network peep/fio2 tables provide the best evidence-based guide to balancing peep and fio2 settings in adults? Respir Care 2007;52(4):461–77.

[35] Koefoed-Nielsen Jacob, Dahlsgaard Nielsen Niels, Kjærgaard Anders J, Larsson Anders. Alveolar recruitment can be predicted from airway pressure-lung volume loops: an experimental study in a porcine acute lung injury model. Crit Care 2008;12(1):R7.

[36] Luecke Thomas, Herrmann Peter, Kraincuk Paul, Pelosi Paolo. Computed tomography scan assessment of lung volume and recruitment during high-frequency oscillatory ventilation. Crit Care Med 2005;33(3):S155–62.

[37] Luecke Thomas, Meinhardt Juergen P, Herrmann Peter, Weiss Andreas, Quintel Michael, Pelosi Paolo. Oleic acid vs saline solution lung lavage-induced acute lung injury: effects on lung morphology, pressure-volume relationships, and response to positive end-expiratory pressure. Chest 2006;130(2):392–401.

[38] Lal Mahto Heera, et al. Year in review 2015: recruitment manoeuvres in ards. Indian Journal of Respiratory Care 2015;4(2). July.

[39] Medoff Benjamin D, Scott Harris R, Kesselman Howard, Venegas Jose, Amato Marcelo BP, Hess Dean. Use of recruitment maneuvers and high positive end-expiratory pressure in a patient with acute respiratory distress syndrome. Crit Care Med 2000;28(4):1210–6.

[40] Nabian Mohsen. Pulmonary pressure-volume data of patients with ards, i) pattern recognition ii) personalization and optimization of mechanical ventilation. 2018. engrXiv.

[41] Nabian Mohsen, Narusawa Uichiro. Quantification of alveolar recruitment for the optimization of mechanical ventilation using quasi-static pressure volume curve. 2018. engrXiv.

[42] Nabian Mohsen, Narusawa Uichiro. Quasi-static pulmonary p–v curves of patients with ards, part i: characterization. Respir Physiol Neurobiol 2018;248:36–42.

[43] Acute Respiratory Distress Syndrome Network. Ventilation with lower tidal volumes as compared with traditional tidal volumes for acute lung injury and the acute respiratory distress syndrome. N Engl J Med 2000;342(18):1301–8.

[44] Acute Respiratory Distress Syndrome Network. Ventilation with lower tidal volumes as compared with traditional tidal volumes for acute lung injury and the acute respiratory distress syndrome. N Engl J Med 2000;342(18):1301–8.

[45] Oba Yuji, Thameem Danish M, Zaza Tareq. High levels of peep may improve survival in acute respiratory distress syndrome: a meta-analysis. Respir Med 2009;103(8):1174–81.

[46] Piacentini Enrique, Wysocki Marc, Blanch Lluis. A new automated method versus continuous positive airway pressure method for measuring pressure–volume curves in patients with acute lung injury. Intensive Care Med 2009;35(3):565–70.

[47] Polak Adam G, Mroczka Janusz. Nonlinear model for mechanical ventilation of human lungs. Comput Biol Med 2006;36(1):41–58.

[48] Poorbahrami Kamran, Oakes Jessica M. Regional flow and deposition variability in adult female lungs: a numerical simulation pilot study. Clin BioMech 2018.

[49] Protti Alessandro, Cressoni Massimo, Santini Alessandro, Langer Thomas, Mietto Cristina, Febres Daniela, Chierichetti Monica, Coppola Silvia, Conte Grazia, Gatti Stefano, et al. Lung stress and strain during mechanical ventilation: any safe threshold? Am J Respir Crit Care Med 2011;183(10):1354–62.

[50] Rouby Jean-Jacques, Ferrari Fabio, Bouhemad Bélaïd, Lu Qin. Positive end-expiratory pressure in acute respiratory distress syndrome: should the'open lung strategy'be replaced by a'protective lung strategy'? Crit Care 2007;11(6):180.

[51] Saini PC, Atina J. Ventilator induced lung injury (vili) in acute respiratory distress syndrome (ards)."barotraumas" to "biotrauma": case report. East Afr Med J 2017;94(5):391–7.

[52] Salazar Eduardo, Knowles John H. An analysis of pressure-volume characteristics of the lungs. J Appl Physiol 1964;19(1):97–104.

[53] Scott Harris R, Hess Dean R, Venegas José G. An objective analysis of the pressure-volume curve in the acute respiratory distress syndrome. Am J Respir Crit Care Med 2000;161(2):432–9.

[54] Shaefi S, Eikermann M. Analysing tidal volumes early after a positive end-expiratory pressure (peep) increase: a new way to determine optimal peep in the operating theatre? 2018.

[55] Sharp JT, Johnson FNEAL, Goldberg NB, Van Lith P. Hysteresis and stress adaptation in the human respiratory system. J Appl Physiol 1967;23(4):487–97.

[56] Slutsky Arthur S, Marco Ranieri V. Ventilator-induced lung injury. N Engl J Med 2013;369(22):2126–36.

[57] Smith Bradford J, Grant Kara A, Bates Jason HT. Linking the development of ventilator-induced injury to mechanical function in the lung. Ann Biomed Eng 2013;41(3):527–36.

[58] Stahl CA, Kuhlen R, Putensen C, Sydow M, Geiger K, Guttmann J. The static pressure–volume curve does not predict the mechanical properties of the respiratory system during mechanical ventilation in acute respiratory distress syndrome (ards) and acute lung injury (ali). Crit Care 2004;8(1):P28.

[59] Suki Béla, Barabási Albert-László, Hantos Zoltán, Peták Ferenc, Eugene Stanley H. Avalanches and power-law behaviour in lung inflation. Nature 1994;368(6472):615.

[60] Sundaresan Ashwath, Yuta Toshinori, Hann Christopher E, Geoffrey Chase J, Shaw Geoffrey M. A minimal model of lung mechanics and model-based markers for optimizing ventilator treatment in ards patients. Comput Meth Progr Biomed 2009;95(2):166–80.

[61] Talmor Daniel, Sarge Todd, Malhotra Atul, O'Donnell Carl R, Ritz Ray, Lisbon Alan, Novack Victor, Loring Stephen H. Mechanical ventilation guided by esophageal pressure in acute lung injury. N Engl J Med 2008;359(20):2095.

[62] Paolo Terragni Pier, Del Sorbo Lorenzo, Mascia Luciana, Urbino Rosario, Martin Erica L, Birocco Alberto, Faggiano Chiara, Quintel Michael, Gattinoni Luciano, Marco Ranieri V. Tidal volume lower than 6 ml/kg enhances lung protectionrole of extracorporeal carbon dioxide removal. Anesthesiology: The Journal of the American Society of Anesthesiologists 2009;111(4):826–35.

[63] Paolo Terragni Pier, Rosboch Giulio, Tealdi Andrea, Corno Eleonora, Menaldo Eleonora, Davini Ottavio, Gandini Giovanni, Herrmann Peter, Mascia Luciana, Quintel Michel, et al. Tidal hyperinflation during low tidal volume ventilation in acute respiratory distress syndrome. Am J Respir Crit Care Med 2007;175(2):160–6.

[64] Tortora Gerard J, Derrickson Bryan H. Principles of anatomy and physiology. John

Wiley & Sons; 2008.

[65] Uzawa Yoshihiro, Otsuji Mikiya, Nakazawa Koichi, Fan Wei, Yamada Yoshitsugu. Derivation of recruitment function from the pressure–volume curve in an acute lung injury model. Respir Physiol Neurobiol 2015;205:16–20.

[66] Venegas José G, Scott Harris R, Simon Brett A. A comprehensive equation for the pulmonary pressure-volume curve. J Appl Physiol 1998;84(1):389–95.

[67] Venegas José G, Scott Harris R, Simon Brett A. A comprehensive equation for the pulmonary pressure-volume curve. J Appl Physiol 1998;84(1):389–95.

[68] Villar Jesús, Blanco Jesús, Kacmarek Robert M. Current incidence and outcome of the acute respiratory distress syndrome. Curr Opin Crit Care 2016;22(1):1–6.

[69] Zannin Emanuela, Dellaca Raffaele L, Kostic Peter, Pompilio Pasquale P, Larsson Anders, Pedotti Antonio, Hedenstierna Goran, Frykholm Peter. Optimizing positive end-expiratory pressure by oscillatory mechanics minimizes tidal recruitment and distension: an experimental study in a lavage model of lung injury. Crit Care 2012;16(6):R217.

Update

Informatics in Medicine Unlocked
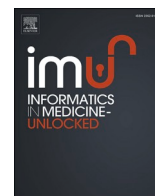
Erratum regarding missing Declaration of Competing Interest statements in previously published articles

Owing to a Publisher error Declaration/Conflict of Interest statements were not included in the published versions of the following articles, that appeared in previous issues of Informatics in Medicine Unlocked.

The appropriate Declaration/Conflict of Interest statements, provided by the Authors, are included below.

1. The relationship between retinal vessel geometrical changes to incidence and progression of Diabetic Macular Edema (Informatics in Medicine Unlocked; 2019; Vol 16C; Article number: 100,248) https://doi.org/10.1016/j.imu.2019.100248

   Declaration of Competing Intere: The Authors have no interests to declare.

2. A machine learning algorithm to improve patient-centric pediatric cardiopulmonary resuscitation (Informatics in Medicine Unlocked; 2020; Vol 19C; Article number: 100,339) https://doi.org/10.1016/j.imu.2020.100339

   Declaration of interest: The Authors have no interests to declare.

3. Decision support system for diagnosing Rheumatic-Musculoskeletal Disease using fuzzy cognitive map technique (Informatics in Medicine Unlocked; 2019; Vol 18C; Article number: 100,279) https://doi.org/10.1016/j.imu.2019.100279

   Declaration of interest: The Authors have no interests to declare.

4. Channel binary pattern based global-local spatial information fusion for motor imagery tasks (Informatics in Medicine Unlocked; 2020; Vol 20C; Article number: 100,352) https://doi.org/10.1016/j.imu.2020.100352

   Declaration of interest: The Authors have no interests to declare.

5. Classification of malignant and benign tissue with logistic regression (Informatics in Medicine Unlocked; 2019; Vol 16C; Article number: 100,189) https://doi.org/10.1016/j.imu.2019.100189

   Declaration of interest: The Authors have no interests to declare.

6. On parameter interpretability of phenomenological-based semi-physical models in biology (Informatics in Medicine Unlocked; 2019; Vol 15C; Article number: 100,158) https://doi.org/10.1016/j.imu.2019.02.002

   Declaration of interest: The Authors have no interests to declare.

7. Multistage Classifier-Based Approach for Alzheimer's Disease Prediction and Retrieval (Informatics in Medicine Unlocked; 2018 vol 14C; Pages 34–42) https://doi.org/10.1016/j.imu.2018.12.003

   Declaration of interest: The Authors have no interests to declare.

8. A novel somatic cancer gene based biomedical document feature ranking and clustering model (Informatics in Medicine Unlocked; 2019; Vol 16C; Article number: 100,188) https://doi.org/10.1016/j.imu.2019.100188

   Declaration of interest: The Authors have no interests to declare.

9. Developing an ultra-efficient microsatellite discoverer to find structural differences between SARS-CoV-1 and Covid-19 (Informatics in Medicine Unlocked; 2020 vol 19C; Article number: 100,356) https://doi.org/10.1016/j.imu.2020.100356

   Declaration of interest: The Authors have no interests to declare.

10. Patient-specific optimization of mechanical ventilation for patients with acute respiratory distress syndrome using quasi-static pulmonary P–V data (Informatics in Medicine Unlocked; 2018;

Vol 12C; Pages 44–55) https://doi.org/10.1016/j.imu.2018.06.003

Declaration of interest: The Authors have no interests to declare.

11. A technology framework for remote patient care in dermatology for early diagnosis (Informatics in Medicine Unlocked; 2019; Vol 15C; Article number: 100,171) https://doi.org/10.1016/j.imu.2019.100171

Declaration of interest: The Authors have no interests to declare.

12. CBIR System Using Capsule Networks and 3D CNN for Alzheimer's disease Diagnosis (Informatics in Medicine Unlocked; 2018; Vol 14C; Pages 59–68) https://doi.org/10.1016/j.imu.2018.12.001

Declaration of interest: The Authors have no interests to declare.

13. The effect of computerized physician order entry on mortality rates in pediatric and neonatal care setting: Meta-analysis (Informatics in Medicine Unlocked; 2020; Vol 19C; Article number: 100,308) https://doi.org/10.1016/j.imu.2020.100308

Declaration of interest: The Authors have no interests to declare.

14. Identification of the core ontologies and signature genes of polycystic ovary syndrome (PCOS): A bioinformatics analysis. (Informatics in Medicine Unlocked; 2020; Vol 18C; Article number: 100,304) https://doi.org/10.1016/j.imu.2020.100304

Declaration of interest: The Authors have no interests to declare.

15. Balanites aegyptiaca (L.) Del. for dermatophytoses: Ascertaining the efficacy and mode of action through experimental and computational approaches (Informatics in Medicine Unlocked; 2019; Vol 15C; Article number: 100,177) https://doi.org/10.1016/j.imu.2019.100177

Declaration of interest: The Authors have no interests to declare.

16. Barriers and technologies of maternal and neonatal referral system in developing countries: A narrative review (Informatics in Medicine Unlocked; 2019; Vol 15C; Article number: 100,184) https://doi.org/10.1016/j.imu.2019.100184

Declaration of interest: The Authors have no interests to declare.

17. Automated Grading of Prostate Cancer using Convolutional Neural Network and Ordinal Class Classifier (Informatics in Medicine Unlocked; 2019; Vol 17C; Article number: 100,256) https://doi.org/10.1016/j.imu.2019.100256

Declaration of interest: The Authors have no interests to declare.